Molecular Vision 2017; 23:572-578 <http://www.molvis.org/molvis/v23/572>
Received 17 January 2017 | Accepted 8 August 2017 | Published 10 August 2017

Magnetic resonance imaging study of eye congenital birth defects in mouse model

Jing-Huei Lee,[1] Zachary Tucker,[1] Maureen Mongan,[2] Qinghang Meng,[2] Ying Xia[2]

[1]Department of Biomedical Engineering, College of Engineering and Applied Science, University of Cincinnati, OH; [2]Department of Environmental Health, College of Medicine, University of Cincinnati, OH

Purpose: Embryonic eyelid closure is a well-documented morphogenetic episode in mammalian eye development. Detection of eyelid closure defect in humans is a major challenge because eyelid closure and reopen occur entirely in utero. As a consequence, congenital eye defects that are associated with failure of embryonic eyelid closure remain unknown. To fill the gap, we developed a mouse model of defective eyelid closure. This preliminary work demonstrates that the magnetic resonance imaging (MRI) approach can be used for the detection of extraocular muscle abnormalities in the mouse model.

Methods: Mice with either normal (*Map3k1*$^{+/-}$) or defective (*Map3k1*$^{-/-}$) embryonic eyelid closure were used in this study. Images of the extraocular muscles were obtained with a 9.4 T high resolution microimaging MRI system. The extraocular muscles were identified, segmented, and measured in each imaging slice using an in-house program.

Results: In agreement with histological findings, the imaging data show that mice with defective embryonic eyelid closure develop less extraocular muscle than normal mice. In addition, the size of the eyeballs was noticeably reduced in mice with defective embryonic eyelid closure.

Conclusions: We demonstrated that MRI can potentially be used for the study of extraocular muscle in the mouse model of the eye open-at-birth defect, despite the lack of specificity of muscle group provided by the current imaging resolution.

In the United States, congenital birth defects of the eye occur in approximately 1 in every 5,000 births [1]. Congenital malformation of the eye and its surrounding tissues can severely impair vision, yet the developmental origin and pathophysiology of these abnormalities remain poorly understood.

Embryonic eyelid closure is an important and well-conserved morphogenetic event in mammalian eye development. The human eyelids are first evident at the 7th week post-fertilization. The upper and lower eyelids fuse to each other at weeks 9−12, and they separate at 4–6 months post-fertilization [2,3]. By analyzing 48 human embryos, Byun and his coworkers showed that while the eyelids are closed, the eyelid and extraocular muscles continue to develop, and the cornea and eyelid appendix structures become mature [3]. These anatomic observations suggest that the transient eyelid closure may facilitate the development of the cornea, ocular muscle, and eyelashes. However, detection of eyelid closure defect is a major challenge because eyelid closure and reopen occur entirely in utero. As a consequence, congenital eye defects that are associated with failure of embryonic eyelid closure have not yet been identified.

Correspondence to: Jing-Huei Lee, 2901 Woodside Drive, 501E ERC, University of Cincinnati, Cincinnati OH 45221-0012; Phone: (513) 558-5676; email: jing-huei.lee@uc.edu

The development of the mouse eyelid also involves a transient closure followed by reopening. Mouse eyelid formation starts at around embryonic day 11.5 (E11.5) when the dorsal and ventral ocular surface ectoderm adjacent to the globe invaginates [4]. Between E15.5 and E16, the epithelium at the eyelid leading edge elongates and migrates, resulting ultimately in fusion of the upper and lower lids [5,6]. The mouse eyelid remains closed between E16.5 and postnatal day (P12−14), and the upper and lower eyelids separate at 2 weeks after birth [5,7]. Although mice are born normally with the lid closed, mice with defective lid closure in embryogenesis exhibit a distinctive eye open-at-birth (EOB) phenotype.

In mice, at least 150 mutant genotypes are associated with the EOB phenotype, and the number is likely to increase with complete or partial knockout of new genes (Mouse Genomic Informatics). In addition, more than 20 spontaneous mutant strains exhibit the defect although the causative genetic factors remain unknown [8]. With the copious genetic resources, the mouse model has become a useful tool for elucidating not only the molecular mechanisms of eyelid morphogenesis but also the congenital eye anomalies associated with defective eyelid development [9].

Previously, we performed histological analyses and identified eyelid, meibomian gland, and extraocular muscle abnormalities in several EOB mutants [9,10]. For example, homozygous mutation of the *Map3k1* gene leads to defective

eyelid closure, but heterozygous mutation of the *Map3k1* gene has no effect on eye development [10,11]. Compared to mice with the heterozygous mutation (*Map3k1*$^{+/-}$), mice with the homozygous (*Map3k1*$^{-/-}$) mutation display truncation of the eyelid tarsal muscles (TM), failure of the levator palpebrae superioris (LPS) extension into the upper eyelid, and misplacement of the inferior oblique (IO) muscle and inferior rectus (IR) muscle (Figure 1) [9].

Magnetic resonance imaging (MRI) has been used for the study of structural and physiologic alterations in the eye and the development of the visual system in small animal models [12-16]. However, to the best of our knowledge, no in vivo imaging study has been applied to extraocular muscle abnormalities in an EOB mouse model. In this study, we verified the differences in ocular muscle between the *Map3k1*$^{+/-}$ and *Map3k1*$^{-/-}$ mice using MRI suitable for clinical diagnosis. We also quantified the volumes of the extraocular muscles and validated that MRI is a valid imaging modality for the viewing and quantification of these muscles. The results provide rationale for future studies to more closely examine the development of extraocular muscles in the mouse model. This work may potentially translate the mouse findings into understanding of human congenital diseases.

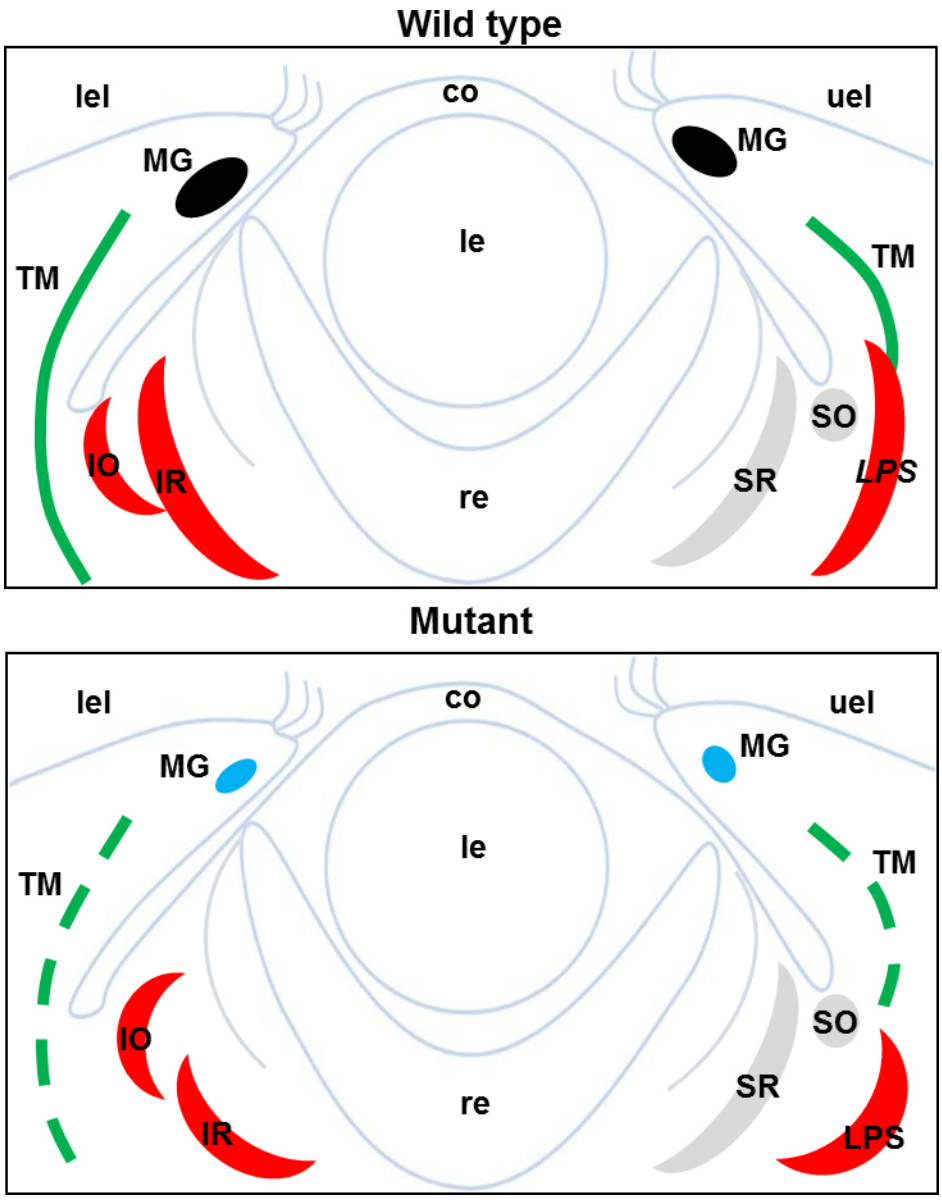

Figure 1. The developmental roles of embryonic eyelid closure. Failure of eyelid closure in embryogenesis causes truncated tarsal muscles, blunted LPS, and abnormal sclera insertion site of the IR muscles. The eye open-at-birth (EOB) mice also develop exposure-driven remodeling changes (bright blue) of the cornea, conjunctiva, and meibomian gland. Lel = lower eyelid, uel = upper eyelid, TM = tarsal muscle, LPS = levator palpebrae superioris, IO = inferior oblique, IR = inferior rectus, SR = superior rectus, SO = superior oblique, MG = meibomian gland, co = cornea, le = lens, re = retina.

METHODS

For proof of the concept, four in-house mice were used in this study. The control group, *Map3k1*$^{+/-}$-1 (HT-1) and *Map3k1*$^{+/-}$-2 (HT-2), had normal eye development; the experimental group, *Map3k1*$^{-/-}$-1 (KO-1) and *Map3k1*$^{-/-}$-2 (KO-2), exhibited the EOB phenotype. All animals were treated in adherence to the Association for Research in Vision and Ophthalmology Statement for the Use of Animals in Ophthalmic and Vision Research and procedures were approved by the Institutional Animal Care and Use Committee at the University of Cincinnati.

The HT-1 and KO-1 mice were female on the B6 background, imaged at P36. HT-2 was a female mouse, and KO-2 was a male mouse, both on the mixed genetic background (129/B6), imaged on P39. The mice imaging was conducted with a Bruker Avance III HD 400-MHz NMR Spectrometer (Billerica, MA) with rodent microimaging capability. The MRI operates at 9.4 T with a wide bore.

Animals were identified with genotyping before being transported from the laboratory animal medical services (LAMS) facility to the scanner room in covered, approved cages. After acclimation for 1–2 h, the animals were anesthetized with up to 5% isoflurane in air (confirmed by toe pinch). The animals were then transferred to the bed of the microimaging probe (anesthesia maintained with 0.5–3% isoflurane in air delivered continuously by nose cone) and secured in the microimaging radiofrequency coil using a bite bar. Body temperature, respiration rate, and pulse oximetry probes were positioned and secured. Ophthalmic ointment was put on the eyes, and the animal further secured with medical tape. The microimaging probe with the secured, anesthetized animal was then inserted into the magnet bore, all external physiologic and electronic lines secured to the probe, warm air flow established through the probe, and isoflurane scavenging set up at the top of the magnet bore.

A scout imaging using a two-dimensional (2D) multislice sequence (TR = 2 s, matrix size = 256 × 256, slice thickness = 3 mm, in plane resolution is 3 × 3 mm^2) was scanned, and then a 3D Tubro RARE spin-echo sequence (TR = 2.5 s, effective TE = 28 ms, matrix size and field of view were adjusted accordingly so that the voxel resolution was about 1.0 × 1.0 × 1.0 mm^3) was performed over a period of about 1 h with continuous isoflurane anesthesia. Warm air flow was adjusted to maintain proper body temperature. Isoflurane concentration was maintained between 0.5% and 3% in air and adjusted as needed to maintain the proper respiration rate, which was used to monitor the depth of the anesthesia. After scanning was complete, the animals were removed from the microimaging probe and were then euthanized with carbon dioxide (inhalation; flow rate 3 litter/min) or an overdose of isoflurane (inhalation, 0.5-5% in air as needed to effect). Euthanasia was confirmed by cervical dislocation.

The muscles were identified in each imaging slice and segmented using the inhomogeneity mapping method outlined by Chen [17]. A brief summary of the method is provided here. For each pixel, the neighborhood surrounding that pixel was defined mathematically. The spatial gradient of a given pixel is then the first derivative of that pixel's image intensity function. The spatial gradient of the neighborhood of pixels surrounding a given pixel can then be defined as the first derivative of the image intensity functions of the neighborhood. The magnitude of all these spatial gradients can thus be determined. In theory, a boundary region is obtained, and optimal local scales allow us to determine the incoherence between two adjacent pixels, which are mutually exclusive neighbors. Once the inhomogeneity of a pixel is determined, it is normalized with the maximum and minimum inhomogeneity values of the image, so that inhomogeneity values can be compared easily across the entire image. These spatial gradient differences can be used to form an inhomogeneity map, which is a matrix of inhomogeneity values for each pixel. The cutoff inhomogeneity can be changed to include more or less discontinuous pixels in a segmentation. After the muscles were segmented, the volume of the muscle was calculated based on the number of pixels the muscle encompassed and the area of each pixel (based on the matrix and the field of view of each image stack).

RESULTS AND DISCUSSION

Figure 2 shows selected images from the MRI image slices showing the automatic segmentation results of the four mice, while Figure 3 illustrates an enlarged section form imaging slice 7 of the HT-1 mouse in Figure 2. Table 1 shows the measured muscle volume of each eye in each mouse. The muscle volume is visibly more abundant in the HT-1 and HT-2 mice than in the KO-1 and KO-2 mice. In addition, the muscles in the HT-1 and HT-2 mice are straighter and more forward in the head of the mouse (Figure 2). In contrast, the muscles in the homozygous mice are warped backward, consistent with previous histological findings (Figure 1) [9]. Furthermore, in the homozygous mice, the inferior rectus and inferior obliques are not layered on top of one another as in the heterozygous mice.

The MRI imaging detected noticeably reduced muscle mass in the homozygous mice compared to their heterozygous counterparts that is in accordance with histological data presented by Meng et al. [9]. They showed that the inferior obliques, inferior rectus, and levator palpebrae superioris are

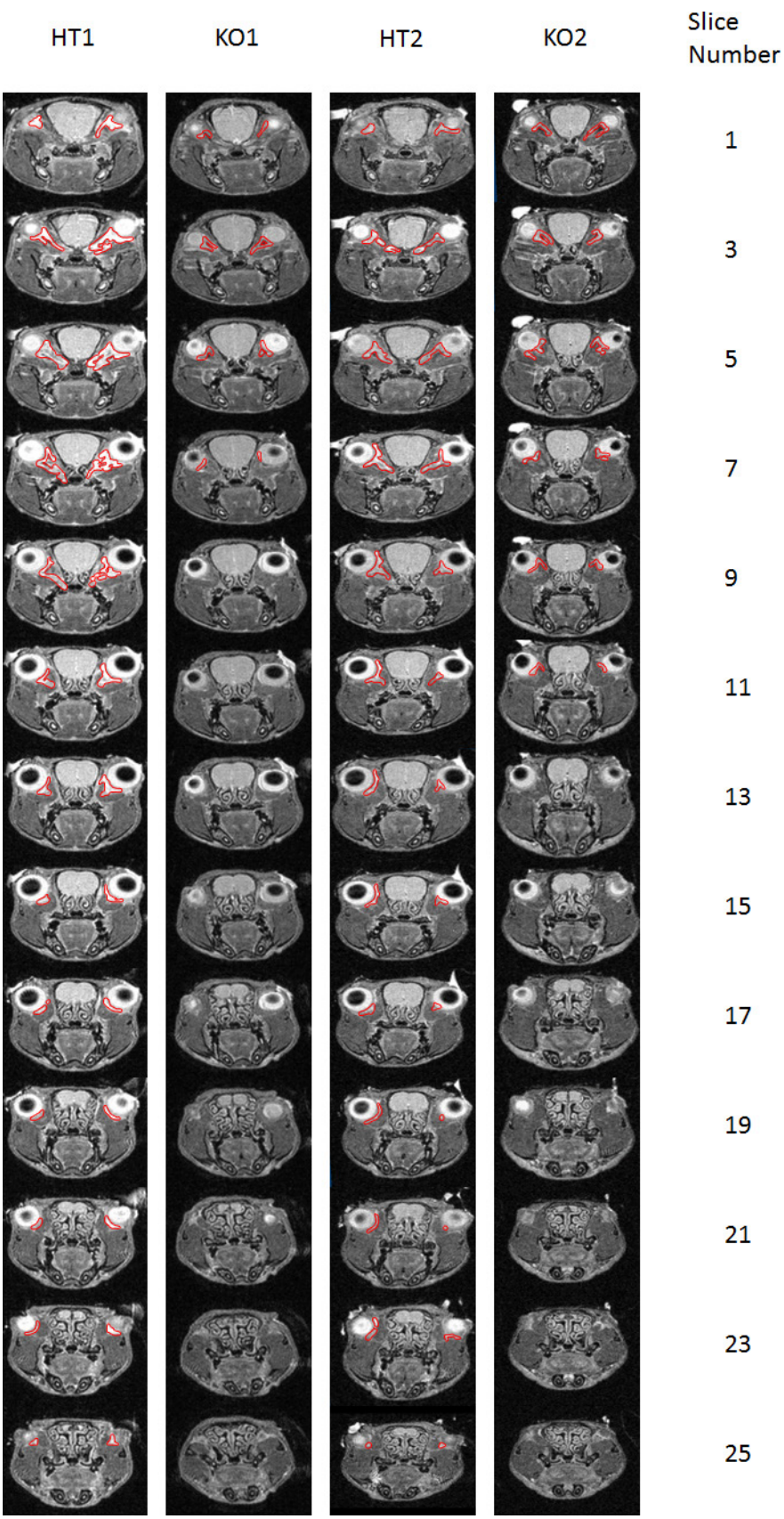

Figure 2. Comparisons of extra-ocular muscles among KO and HT mice. Selected coronal image slices for four mice: two KO (knockout) and two HT (wild-type) mice. The image slice is arranged from posterior to anterior when the slice number increases from small to large. The red lines are the automatic segmentation results using in-house software. The in-pane resolution is 1.0 by 1.0 mm^2, and the slice thickness is 1.0 mm.

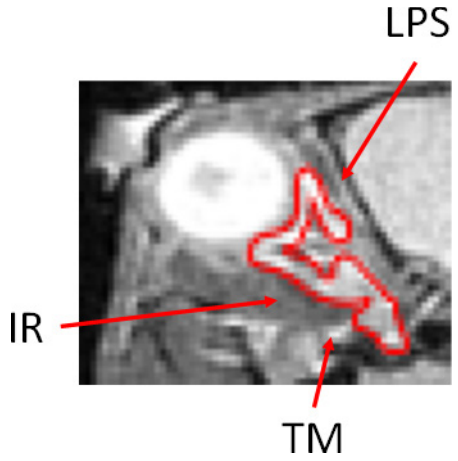

Figure 3. An enlarged image from slice 7 of HT-1 in Figure 2. The zoom image illustrates that the software can identify the extraocular muscles as a whole but cannot differentiate among them due to imaging resolution limitations.

all smaller in the homozygous compared with the heterozygous mice. In the present work, the locations of the inferior oblique, inferior rectus, and levator palpebrae superioris were inferred empirically and based on the MRI images of the mice. As shown in Figure 3, the MRI images did not provide sufficient resolution to differentiate between the muscle groups, and we were unable to measure each muscle individually. Thus, these data could not exclude the possibility that only one of the relevant muscle groups was truncated, warped, or displaced while the others were the same size in the heterozygous and homozygous mice. Even if this were the case, there is still a noticeable phenotypic difference between the two groups of mice. Whether there is a statistically significant difference between these two groups can be determined only after examination of a larger group of mice.

Unlike previous histological studies [9], we were unable to observe the tarsal muscles, likely because the muscles were too small to be detected with the current MRI setting. Moreover, the close proximity of these muscles to the eyeball might increase the difficulties of their detection. Despite the limitations, the MRI imaging modality provides sufficient resolution to observe the sizes of the muscles versus surrounding tissue and provides pivotal confirmation of the histological data [9], showing muscle abnormalities in mice with defective eyelid development.

Table 1. Comparisons of volumes of extraocular muscles.

Mouse	Eye	Volume (mm3)
HT1	Left	4.22
HT1	Right	4.78
KO1	Left	0.85
KO1	Right	0.49
HT2	Left	1.82
HT2	Right	1.48
KO2	Left	0.71
KO2	Right	0.78

Despite the lack of specificity provided by the MRI modality, MRI can be useful for the study of muscle abnormalities in the EOB mouse model. With MRI, three-dimensional structures are adequately observed. The truncated, volume-reduced, and displaced muscles can be observed in the KO mice, suggesting that developmental eyelid closure is required for proper extension and position of extraocular muscles. This observation is consistent with the notion that eyelid morphogenesis is associated with the development of the ocular adnexa [9]. Pinpointing the EOB-specific abnormalities of the extraocular muscle, however, is still challenging, and certainly requires better improved imaging resolution, a larger sample size, and expanded EOB strains with the inclusion of additional genetic mutants.

The size of the eyeballs themselves was noticeably reduced in the homozygous mice. The size of the eyeballs also varied with respect to each other in a particular homozygous mouse. In the KO-1 mouse, the left eye was significantly smaller than the right eye, and in the KO-2 mouse, the right eye was shifted posteriorly compared to the left eye. It has yet to be determined whether the smaller eyeball is due to impairment of lens development by either a gene mutation or secondary effects of the EOB defect. The EOB defect has been associated with a smaller lens in several mouse models. In addition, when an EOB defect occurs, the eye is left exposed to the environment as the eye continues to develop ex vivo, and the damage that occurs to the eye during this time can be observed with the MRI modality as well. Applying the imaging tool developed here on prenatal or neonatal pups, as we have done with the histological analyses [9], would likely eliminate any secondary effects caused by environmental exposure.

The use of high-resolution MRI is sufficient to determine the size of the ocular musculature, which is validated against previous data by comparing the measured size of the eye to that of the actual eye. Using the current MRI approach, the methodology was sufficient to detect the difference in size of the ocular musculature as a whole, but not the individual muscle groups. It was also difficult in some cases to determine where the musculature and tendons differed in location. Despite this, MRI appears to be a sufficient modality for the characterization of phenotype versus genotype in a mouse model, although with less specificity than histological

analysis. The benefit of being able to use MRI in vivo potentially offsets this loss in precision.

Defects of eye development lead to congenital malformation of the eye, affecting 1 in 2,000 newborns. The etiology is largely under-explored. The imaging (Figure 2) data presented here are consistent with previous histological analyses and suggest that defective eyelid closure in embryogenesis may perturb the formation of eye and its surrounding tissues causing congenital eye diseases. The diseases likely have complex etiology, as we have shown that eyelid closure defects in mice are induced by multiple genetic lesions involving gene–gene and gene–environment interactions [18-20]. Although a link between eyelid closure problems with congenital eye disorders has yet to be established, there are cases where genetic mutations affecting embryonic eyelid development in mice have been found to also be mutated in humans with birth defects of the eye. For example, the mutation in *FOXL2* (Gene ID 668; OMIM 605597) is associated with blepharophimosis, ptosis, epicanthus-inversus syndrome (BPES), characterized by abnormalities of the eyelids, such as blepharophimosis, ptosis, epicanthus inversus, and telecanthus [21,22]. Likewise, *Foxl2*-null mice display craniofacial dysmorphic features comparable to BPES, involving severe eyelid hypoplasia, necrotizing eyes, and the EOB phenotype [23]. Mutations in the porcupine (*PORCN*; Gene ID 64840; OMIM 300651) gene are associated with focal dermal hypoplasia (FDH) with microphthalmos as a common eye manifestation [24]. Correspondingly, deletion of PORCN in ocular tissues during mouse development leads to severe eye abnormalities, including coloboma, defective optic cup periphery, defective corneal morphogenesis, as well as the EOB phenotype. Mutations of genes in the *FRAS* (OMIM 300651) and *FREM* (OMIM 608946) family are associated with Fraser's syndrome (FS) and Manitoba-oculo-tricho-anal (MOTA) syndrome, the eye phenotype of which includes eyelid colobomas, cryptophthalmos, and anophthalmia/microphthalmia [25,26]. Accordingly, *Fras1*-, *Frem1*-, and *Frem2*-deficient mice display eye malformations, such as complete fusion of one or both eyelids, highly comparable to those featured in patients with Fraser syndrome [27]. Whether the failure of eyelid closure contributes to any of the disease phenotypes is still an open question, because the gene mutations affect multiple developmental processes in addition to the eyelids.

The MRI modality reported here does not appear to provide sufficient resolution to make measurements of specific muscle groups; however, it does appear to be sufficient to characterize whether an EOB defect has occurred in a mouse model. Potential next steps for validation of the use of MRI in a mouse model are the addition of more mice to the sample group with diverse genetic conditions and younger ages, use of different MRI parameters to allow for greater precision (to determine the sizes and shapes of specific muscle groups), and application of morphometrics to quantify the shape of the wild-type and mutated muscles. The ultimate goal is to establish the MRI imaging profile of ocular abnormalities associated with defective embryonic eyelid closure. Information derived in the mouse models may be applied to the analyses of human MRI data to understand the molecular and developmental basis of human congenital eye diseases.

ACKNOWLEDGMENTS

Authors would to thank Ms. Elizabeth Fugate for her assisting in imaging data collection. We also thank National Institutes of Health (NEI RO1EY15227) for supporting this work.

REFERENCES

1. "Data and Statistics." Birth Defects. Centers for Disease Control and Prevention, 29 Feb. 2016. Web. 1 Mar. 2016. <http://www.cdc.gov/ncbddd/birthdefects/data.html#modalIdString_table-Nattional-Estimates>.
2. Doxanas MT, Anderson RL. Oriental eyelids: An anatomic study. Arch Ophthalmol 1984; 102:1232-5. [PMID: 6466190].
3. Byun TH, Kim JT, Park HW, Kim WK. Timetable for upper eyelid development in staged human embryos and fetuses. Anat Rec (Hoboken) 2011; 294:789-96. [PMID: 21416630].
4. Tao H, Ono K, Kurose H, Noji S, Ohuchi H. Exogenous FGF10 can rescue an eye-open at birth phenotype of Fgf10-null mice by activating activin and TGFalpha-EGFR signaling 1. Dev Growth Differ 2006; 48:339-46. [PMID: 16759284].
5. Findlater GS, McDougall RD, Kaufman MH. Eyelid development, fusion and subsequent reopening in the mouse. J Anat 1993; 183:121-9. [PMID: 8270467].
6. Harris MJ, McLeod MJ. Eyelid growth and fusion in fetal mice. A scanning electron microscope study. Anat Embryol (Berl) 1982; 164:207-20. [PMID: 7125235].
7. Mohamed YH, Gong H, Amemiya T. Role of apoptosis in eyelid development. Exp Eye Res 2003; 76:115-23. [PMID: 12589781].
8. Juriloff DM, Harris MJ, Miller JR. The lidgap defect in mice: update and hypotheses. Can J Genet Cytol 1983; 25:246-54. [PMID: 6883178].
9. Meng Q, Mongan M, Carreira V, Kurita H, Liu CY, Kao WW, Xia Y. Eyelid closure in embryogenesis is required for ocular adnexa development. Invest Ophthalmol Vis Sci 2014; 55:7652-61. [PMID: 25377219].
10. Yujiri T, Ware M, Widmann C, Oyer R, Russell D, Chan E, Zaitsu Y, Clarke P, Tyler K, Oka Y, Fanger GR, Henson P, Johnson GL. MEK kinase 1 gene disruption alters cell migration and c-Jun NH2-terminal kinase regulation but does not

cause a measurable defect in NF-kappa B activation. Proc Natl Acad Sci USA 2000; 97:7272-7. [PMID: 10852963].

11. Zhang L, Wang W, Hayashi Y, Jester JV, Birk DE, Gao M, Liu CY, Kao WW, Karin M, Xia Y. A role for MEK kinase 1 in TGF-beta/activin-induced epithelium movement and embryonic eyelid closure. EMBO J 2003; 22:4443-54. [PMID: 12941696].
12. Wang J, Call M, Mongan M, Kao WW, Xia Y. Meibomian gland morphogenesis requires developmental eyelid closure and lid fusion. Ocul Surf 2017; S1542:30015-0. [PMID: 28284825].
13. Chan KC, Xing KK, Cheung MM, Zhou IY, Wu EX. Functional MRI of postnatal visual development in normal and hypoxic–ischemic-injured superior colliculi. Neuroimage 2010; 49:2013-20. [PMID: 19879366].
14. Tkatchenko TV, Shen Y, Tkatchenko AV. Analysis of postnatal eye development in the mouse with high-resolution small animal magnetic resonance imaging. Invest Ophthalmol Vis Sci 2010; 51:21-7. [PMID: 19661239].
15. Chan KC, Cheng JS, Fan S, Zhou IY, Yang J, Wu EX. In vivo evaluation of retinal and callosal projections in early postnatal development and plasticity using manganese-enhanced MRI and diffusion tensor imaging. Neuroimage 2012; 59:2274-83. [PMID: 21985904].
16. Chan KC, Kancherla S, Fan S, Wu EX. Long-term effects of neonatal hypoxia-ischemia on structural and physiological integrity of the eye and visual pathway by multimodal MRI. Invest Ophthalmol Vis Sci 2015; 56:1-9. [PMID: 25491295].
17. Chen K. Adaptive smoothing via contextual and local discontinuities. IEEE TPAMI 2002; 27:1552-67. [PMID: 16237991].
18. Mongan M, Meng Q, Wang J, Kao WW, Puga A. Xia. Gene-environment interactions target mitogen-activated protein 3 kinase 1 (MAP3K1) signaling in eyelid morphogenesis. J Biol Chem 2015; 290:19770-9. [PMID: 26109068].
19. Geh E, Meng Q, Mongan M, Wang J, Takatori A, Zhang Y, Puga A, Lang RA, Xia Y. Mitogen-activated protein kinase kinase kinase 1 (MAP3K1) integrates developmental signals for eyelid closure. Proc Natl Acad Sci USA 2011; 108:17349-54. [PMID: 21969564].
20. Takatori A, Geh E, Chen L, Zhang L, Meller J, Xia Y. Differential transmission of MEKK1 morphogenetic signals by JNK1 and JNK2. Development 2008; 135:23-32. [PMID: 18032450].
21. Crisponi L, Deiana M, Loi A, Chiappe F, Uda M, Amati P, Bisceglia L, Zelante L, Nagaraja R, Porcu S, Ristaldi MS, Marzella R, Rocchi M, Nicolino M, Lienhardt-Roussie A, Nivelon A, Verloes A, Schlessinger D, Gasparini P, Bonneau D, Cao A, Pilia G. The putative forkhead transcription factor FOXL2 is mutated in blepharophimosis/ptosis/epicanthus inversus syndrome. Nat Genet 2001; 27:159-66. [PMID: 11175783].
22. Heude É, Bellessort B, Fontaine A, Hamazaki M, Treier AC, Treier M, Levi G, Narboux-Nême N. Etiology of craniofacial malformations in mouse models of blepharophimosis, ptosis and epicanthus inversus syndrome. Hum Mol Genet 2015; 24:1670-81. [PMID: 25416281].
23. Uda M, Ottolenghi C, Crisponi L, Garcia JE, Deiana M, Kimber W, Forabosco A, Cao A, Schlessinger D, Pilia G. Foxl2 disruption causes mouse ovarian failure by pervasive blockage of follicle development. Hum Mol Genet 2004; 13:1171-81. [PMID: 15056605].
24. Bankhead EJ, Colasanto MP, Dyorich KM, Jamrich M, Murtaugh LC, Fuhrmann S. Multiple requirements of the focal dermal hypoplasia gene porcupine during ocular morphogenesis. Am J Pathol 2015; 185:197-213. [PMID: 25451153].
25. Chacon-Camacho OF, Zenker M, Schanze D, Ledesma-Gil J, Zenteno JC. Novel FREM1 mutations in a patient with MOTA syndrome: Clinical findings, mutation update and review of FREM1-related disorders literature. Eur J Med Genet 2017; 60:190-4. [PMID: 28111185].
26. Jadeja S, Smyth I, Pitera JE, Taylor MS, van Haelst M, Bentley E, McGregor L, Hopkins J, Chalepakis G, Philip N, Perez Aytes A, Watt FM, Darling SM, Jackson I, Woolf AS, Scambler PJ. Identification of a new gene mutated in Fraser syndrome and mouse myelencephalic blebs. Nat Genet 2005; 37:520-5. [PMID: 15838507].
27. Petrou P, Makrygiannis AK, Chalepakis G. The Fras1/Frem family of extracellular matrix proteins: structure, function, and association with Fraser syndrome and the mouse bleb phenotype. Connect Tissue Res 2008; 49:277-82. [PMID: 18661360].

Articles are provided courtesy of Emory University and the Zhongshan Ophthalmic Center, Sun Yat-sen University, P.R. China. The print version of this article was created on 10 August 2017. This reflects all typographical corrections and errata to the article through that date. Details of any changes may be found in the online version of the article.